PHYSICAL REVIEW C VOLUME 48, NUMBER 2 AUGUST 1993

Transition from complete to incomplete fusion in asymmetric heavy ion reactions

K. Hanold, L. G. Moretto, G. F. Peaslee,* and G. J. Wozniak
Nuclear Science Division, Lawrence Berkeley Laboratory, Berkeley, California 94720

D. R. Bowman,† M. F. Mohar,‡ and D. J. Morrissey
National Superconducting Cyclotron Laboratory, Michigan State University, East Lansing, Michigan 48824

(Received 13 January 1993)

Complex fragments with atomic numbers between those of the target and the projectile have been detected from the reactions of 26 and 31 MeV/nucleon ^{129}Xe + C, Al, Ti, and Cu. Angular distributions, cross sections, and velocity spectra of these fragments were extracted from the inclusive data. The velocity of the emitting source and Z-total distributions were reconstructed from the twofold coincidence data. These results are used to characterize the emission source of the complex fragments. The results are compared to a geometric incomplete fusion model calculation. Agreement between the model and the data is good.

PACS number(s): 25.70.Gh, 25.70.Jj

I. INTRODUCTION

The characterization of the source of complex fragments ($Z > 3$) in heavy ion induced reactions is presently of great interest. Complex fragment (CF) emission has been observed at both low [1–8] and intermediate [9–31] bombarding energies for a wide variety of reaction systems. Two sources of complex fragments have been observed, a "nonequilibrium" source that is characterized by forward peaked angular distributions in normal kinematic reactions [9, 10, 32] and a second, "equilibrium" source that is characterized by Coulomb-like velocities and $1/\sin\theta$ angular distributions in the center-of-mass frame [4–10]. This second source has been shown [33] to come mainly from the statistical decay of an excited compound nucleus (CN) formed in either fusion, or, at larger bombarding energies, an incomplete fusion process.

CF emission from excited compound nuclei has been systematically studied for asymmetric entrance channels (X + C and Al), where X ranges across the Periodic table. At bombarding energies below $\approx$10 MeV/nucleon, CF emission by the CN is rare [1–3,7]. This is due to the low excitation energy attained in these near Coulomb barrier bombarding energies. However, as the bombarding energy is increased, the maximum excitation energy increases and the probability of CF emission rises rapidly [4–7,9,10].

For asymmetric entrance channels reactions at low (E/A<20 MeV) bombarding energies, many of the features of the "equilibrium" CF production are quantitatively described [4–7] by assuming a complete fusion reaction mechanism and then calculating the decay of the resulting CN using the statistical decay code GEMINI [4]. However, this statistical approach fails to reproduce the data from asymmetric systems at higher (E/A>35 MeV) bombarding energies [21, 22, 34, 35]. If this failure is due to the change of reaction mechanism from complete to incomplete fusion, one should use an incomplete fusion model to describe the production of the primary fragments as a function of impact parameter rather than the complete fusion model. The primary fragments could then be used as the starting point for a statistical model calculation describing their decay.

Studies of more symmetric reaction systems exhibit a more complicated picture [8, 22, 34, 35]. CF's are no longer associated with a single source, but rather with a broad range of sources. A study [8] of the 18 MeV/nucleon ^{139}La + Ni reaction concluded that this broad distribution of sources is produced by an incomplete fusion process. Incomplete fusion leads to different mass transfers as a function of impact parameter, producing CN with systematically varying masses, excitation energies, and angular momenta. By selecting a given source velocity, it was possible to characterize the product formed in a specific incomplete fusion process and its decay.

In the present work we report on the results for CF emission from the reactions of ^{129}Xe at 26 and 31 MeV/nucleon with targets of C, Al, Ti, and Cu. By using reverse kinematics rather than normal kinematics, the fragments have a larger kinetic energy, so that they are easily detected and identified in $\Delta E - E$ telescopes. However, since in reverse kinematics the fragments are forward focused, heavy fragments can be lost as they are concentrated at small angles near the beam and careful position measurements must be made to extract angular distributions. Data were taken at two energies intermediate to those used in the previous studies [6,8,22], so that the transition from complete fusion to incomplete fusion

---

*Present address: National Superconducting Cyclotron Laboratory, Michigan State University, East Lansing, MI 48824.

†Present address: Nuclear Physics Branch, Chalk River Laboratory, Chalk River, Ontario, Canada K0J 1J0.

‡Present address: Nuclear Science Division, Lawrence Berkeley Laboratory, Berkeley, CA 94720.

could be examined. Four targets were used so that the effect of varying the entrance channel asymmetry could be studied. In the present study, we compared the data with the results from a model using incomplete fusion to simulate the first stage of the reaction and then, in the second stage, we used a statistical decay code to simulate the deexcitation of the excited fragments from the incomplete fusion process.

II. EXPERIMENT

Beams of 26 MeV/nucleon ^{129}Xe^{22+} and 31 MeV/nucleon ^{129}Xe^{23+} produced by the K1200 cyclotron at the National Superconducting Cyclotron Laboratory at Michigan State University were reacted with thin targets of ^{12}C (1.0 mg/cm^2), ^{27}Al (2.0 mg/cm^2), $^{\rm nat}$Ti (2.2 mg/cm^2), and $^{\rm nat}$Cu (2.9 mg/cm^2). The K1200 cyclotron provided beam intensities of approximately 0.2 pnA. The detection apparatus consisted of eight detector telescopes arranged in a plane with four telescopes on either side of the beam. Each telescope consisted of a gas ΔE section, and a 5 mm Si(Li) E, and was position sensitive in two dimensions. These detectors have been described elsewhere [4] and are similar in design to earlier gas ΔE/Si E heavy ion telescopes [36]. Low intensity beams of ^{12}C^{2+}, ^{36}Ar^{6+}, ^{84}Kr^{14+}, and ^{129}Xe^{22+} at 26 MeV/nucleon and ^{129}Xe^{23+} at 31 MeV/nucleon were directed into each detector for calibration purposes. The filling gas was carbon tetrafluoride and was maintained at a pressure of 30 torr. The gas ΔE segment was calibrated by measuring the difference in the energy deposited in the Si detector with and without the gas in the detector. The overall error in the energy calibration of each detector is estimated to be 1% and individual Z values were resolved up $Z =$ 30. The vertical position was measured by the drift time in the gas chamber and the horizontal position by resistive division of the Si(Li) signal. The position spectrum was calibrated using a 49-hole mask which could be remotely placed in front of the telescope. The total in- and out-of-plane coverage was 25° and 10°, respectively.

III. RESULTS AND DISCUSSION

A. Source and emission velocities

In general, the characterization of the source of CF's is a complex problem. However, for very asymmetric reactions, the problem is easier as one typically observes a single source. If one plots the velocity distribution for the CF's from a very asymmetric reaction in the $V_{\|}$-$V_{\perp}$ plane, one observes a circular ring of approximately constant $\partial^2\sigma/\partial V_{\|}\partial V_{\perp}$ for each Z value. The radius of this ring is related to the Coulomb repulsion of the emitted fragments. Moreover, if the yield along the circumference of the ring is isotropic in $d\sigma/d\theta$, this is an indication of a long-lived source that had undergone binary decay. Thus, plots of the distribution of fragment velocities in the $V_{\|}$-$V_{\perp}$ plane can give valuable information on the reaction process.

In order to identify the source, or sources, of CF's in these reactions, the observed kinetic energy distributions should be transformed into velocity distributions. However, the mass of the fragment was not directly measured and a transformation from Z to mass is required. The velocity of each fragment was determined using the measured kinetic energy and Z value by assuming that the mass is given by

$$A = 2.08Z + 0.029Z^2. \tag{1}$$

This expression is valid for heavy nuclei that have undergone extensive evaporation [4]. From the calculated velocity and the measured scattering angle, a distribution of $\partial^2\sigma/\partial V_{\|}\partial V_{\perp}$ was generated for each atomic number. The limited out-of-plane acceptance was accounted for by calculating the fraction of the out-of-plane angles covered at a particular θ angle and then multiplying the data at that angle by the reciprocal of the fraction subtended. The out-of-plane acceptance at a particular θ angle ranged from 17% at small angles to 3% at large angles. Some representative double differential velocity distributions are shown in Figs. 1 and 2 for the reactions at 26 MeV/nucleon and 31 MeV/nucleon, respectively. (The distributions for the reactions at 31 MeV/nucleon are incomplete due to an incomplete coverage of the laboratory angular range.) The data have been made symmetric about the beam and smoothed to aid presentation. For the very asymmetric ^{129}Xe + C and Al reactions, these distributions show well-defined rings for all Z values. These rings (also observed in numerous reactions at lower energies [4, 6, 8]) represent evidence for the emission of fragments with fixed average energies from a fixed longitudinal velocity source. For most Z values, the intensity along the circumference of the ring is fairly uniform. However, the smaller fragments show a backward peaking, which, at lower bombarding energies, has been associated with a targetlike deep-inelastic component [4]. For the heavier targets, rings are no longer observed. A broader range of source velocities, possibly populated by incomplete fusion processes, leads to the smearing of the rings along $V_{\|}$.

The center of a ring defines the average laboratory velocity of the emitting source, and its radius defines the velocity with which the fragments are emitted from that source. In those cases in which a ring could be observed, its center was determined by assuming that the center of the circle was on the line of the beam velocity. First, a spectrum was created for a cut through the ring at small $V_{\perp}$. The resulting spectrum contained two peaks, corresponding to the forward and backward emitted fragments. Each of these peaks was then fit to a Gaussian function and the average of the two centroids was taken as the source velocity of that ring. This procedure was applied to the data for Xe + C, Al, Ti, and Cu reactions at 26 MeV/nucleon and Xe + C and Al reactions at 31 MeV/nucleon. At the higher bombarding energy, the determination of the source velocity for the heavier systems becomes highly uncertain due to the large width of the rings. The rings for the high Z values from the lower bombarding energy are also subject to this limitation. The source velocities extracted with this procedure are shown in Fig. 3 as a function of the fragment Z value for the different targets. The variation of the ex-

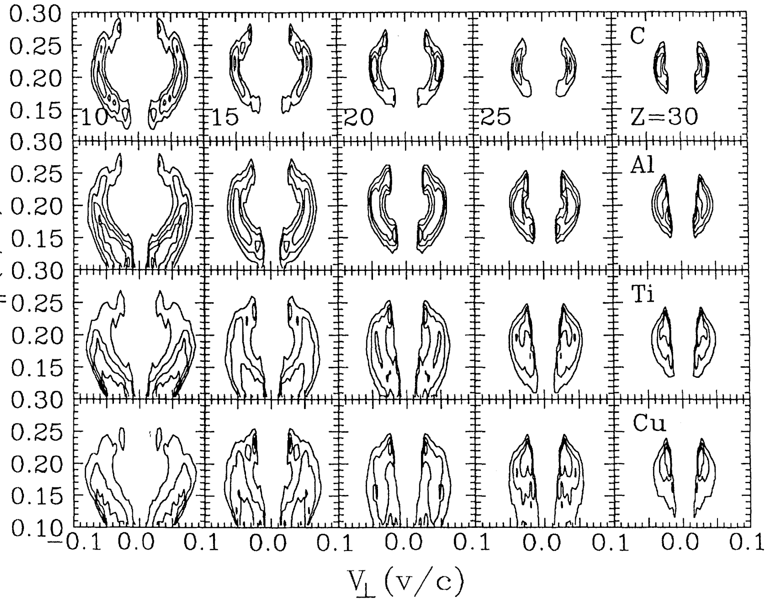

FIG. 1. Linear contours of the experimental cross sections $\partial^2\sigma/\partial V_\parallel\,\partial V_\perp$ in the $V_\parallel$-$V_\perp$ plane for representative Z values produced in reactions of 26 MeV/nucleon ^{129}Xe + C (top row), Al (2nd row), Ti (3rd row) and Cu (bottom row) for representative Z values [10,15,20,25,30]. The Z value is noted in the lower left-hand corner of each column. (The beam direction is vertical.) The data have been smoothed and symmetrized to aid in presentation.

tracted source velocity with the Z value of the fragment is fairly small and is only slightly larger than the error in the determination of the source velocity. In addition, these values are generally in agreement with the value extracted from the coincidence data (dashed line) that will be discussed below. The arrows on the left-hand side of Fig. 3 indicate the complete fusion velocity of each system. Notice that the very asymmetric ^{129}Xe + C and Al systems have average source velocities that are consistent with complete fusion to within the error of the measurement. At 31 MeV/nucleon, the average source velocity for the ^{129}Xe + C reactions is slightly below the complete fusion velocity. However, this difference is within the error of the measurement and might be attributed to a small systematic error in the energy calibration. On the other hand, the more symmetric ^{129}Xe + Ti and Cu systems have average source velocities that are somewhat greater than that for complete fusion.

The laboratory kinetic energies and angles were converted from the laboratory frame into the average moving source frame for each reaction. The resulting moving source frame data were then binned into equal size $\Delta\theta$ bins for the angular distributions and the source-frame, emission-velocity distributions were also determined. The mean emission velocity for each atomic number and the width of each distribution are shown in Fig. 4. Note the almost linear decrease in the transformed emission velocity with increasing emitted frag-

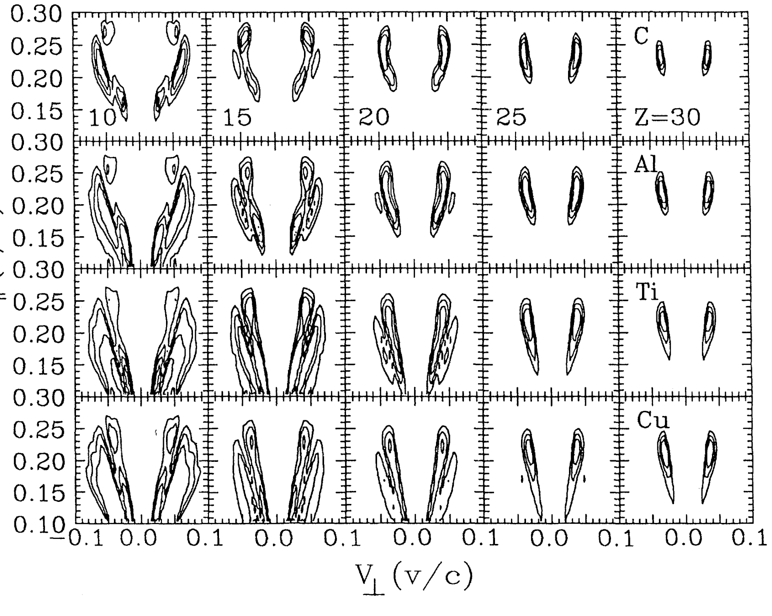

FIG. 2. Same as Fig. 1 but for 31 MeV/nucleon ^{129}Xe induced reactions. The gaps in the distributions are caused by an incomplete coverage of the laboratory angular distribution.

ment charge. This nearly linear decrease is consistent with the expectation that the velocity is mainly determined by the Coulomb repulsion of the fragment and its decay partner [4]. Also, the source frame emission velocity for a particular Z value is almost constant, independent of the target or bombarding energy. This suggests that the nuclear charge, Z, of the source is nearly constant. In contrast, the widths of the transformed emission velocity increase as the target becomes larger. This is expected for increasing center-of-mass energies for the larger systems (see Table I). For large excitation energies, the primary products of the binary decay are hotter and undergo more extensive evaporation which broadens the emission-velocity distributions. The uncertainties in the mean and the width of the emission-velocity distributions are about the size of the symbols in Fig. 4. The smaller Z fragments are not shown due to the limited laboratory angular range measured.

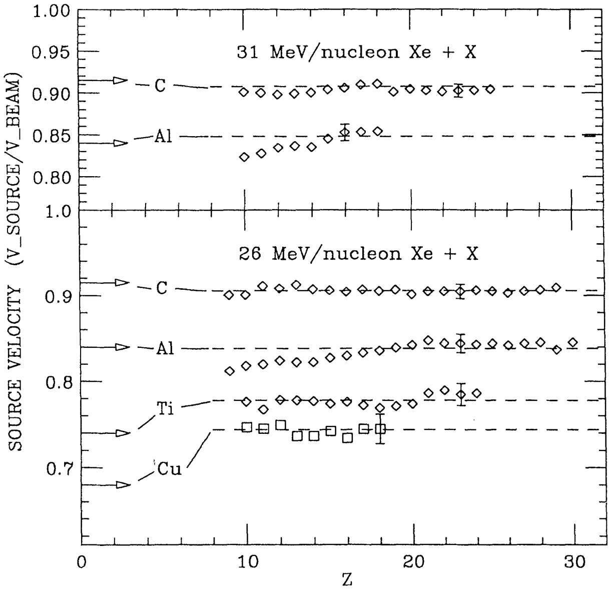

FIG. 3. Source velocities (plot symbols) as a function of a fragment Z value for the reactions at 26 MeV/nucleon (top) and 31 MeV/nucleon (bottom). The error bars shown for the Ti and Cu data indicate the possible error due to the width of the rings. The dashed line represents the source velocity extracted from the twofold coincidence events for each system. The arrows at the left edge of the figure indicate the center-of-mass velocity for the 31 MeV/nucleon ^{129}Xe + C and Al reactions in the top part of the figure and 26 MeV/nucleon ^{129}Xe + C, Al, Ti, and Cu reactions in the bottom part. Note the suppressed zero on the ordinate axis.

B. Angular distributions

Typical angular distributions of the fragments in the source frame are shown in Figs. 5 and 6. For the very asymmetric ^{129}Xe + C systems, the angular distributions are approximately constant in $d\sigma/d\theta$, as expected for the isotropic emission of fragments, for a wide range of Z values intermediate between the projectile and target. In other words, the distributions have a $d\sigma/d\Omega \propto 1/\sin\theta$ form indicating isotropic emission in the reaction plane. Such distributions have been observed previously at 14 and 18 MeV/nucleon [6] for a very similar system (^{139}La + C). For the lightest fragments (Z <10), the angular distributions are backwards peaked. (The light fragments are spread over a large angular range. Due to the limited beam time, fragments at laboratory angles larger than 25° were not measured and therefore the light fragment distributions are incomplete and are not shown.) Such a backward-peaked component in the the angular distributions has been previously associated [6] with targetlike fragments at low Z values. This backward peaking must be associated with a corresponding forward peaking at high Z values from the projectilelike fragments. These effects are presumed to arise from deep-inelastic processes. Similar distributions have been seen at both lower [4, 6] and higher energies [22,

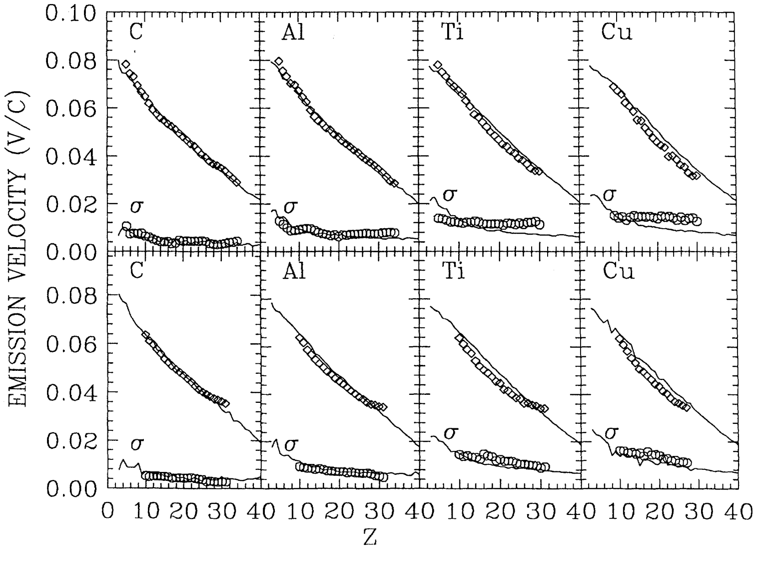

FIG. 4. Mean emission velocities (diamonds) measured at 90° in the source frame as a function of a fragment Z value. The top row is for the reaction of 26 MeV/nucleon ^{129}Xe and the bottom row is for 31 MeV/nucleon ^{129}Xe. The targets are indicated in the upper left of each panel. At the bottom of the panel for each system are the widths (circles) of the emission velocity distributions at 90° in the source frame. The solid lines correspond to the predictions of the mean value and the width of the emission velocity distributions from the GEMINI calculations.

27, 34, 35]. The angular distributions from reactions in the slightly more symmetric ^{129}Xe+Al reaction are also similar. However, the anisotropy observed for large and small fragments is more pronounced and the range of atomic numbers whose angular distributions are isotropic is more restricted. For the heaviest systems, the backward peaking present at low Z values decreases making a transition, around Z=25, to forward-peaked distributions which become even more forward peaked as the Z value increases. The angular distributions for the 31 MeV/nucleon reactions, shown in Fig. 6, are very similar to the angular distributions from the 26 MeV/nucleon data and are also similar to those distributions reported for higher bombarding energies [22, 35, 34].

C. Integrated cross sections

The individual angular distributions were integrated to extract the fragment cross section for each atomic number. The integration was performed by fitting a quadratic function to the angular distribution and then integrating it over the full angular range. The fitted functions are shown as solid lines on the angular distribution figures (Figs. 5 and 6) and the integrated cross sections are shown in Fig. 7. The statistical error in the cross section values is smaller than the plotting symbol, about 5%, however, the systematic errors may be as large as 30%. The sources of the systematic errors are about 10% from the beam current and target thickness, and 10% for the lighter fragments to 20% for the heavy fragments from the angular distribution integration procedure. The total cross section increases rapidly with increasing target mass, and is correlated with the available center-of-mass energy (Table I). The cross sections are consistent with the values obtained for similar systems at energies both above and below the present beam energy [4, 6, 22, 34, 35]. The charge distribution for the reaction of ^{129}Xe+C at 26 MeV/nucleon, as a function of increasing Z value, decreases strongly at small Z values, going through a minimum at Z = 18 and then peaks at Z = 30. Such minimum and peak values are barely visible with the slightly heavier Al target that also has a shoulder in the Z = 10–15 region. This shoulder has been observed at higher bombarding energies and was attributed to multibody events [22]. For the heavier targets, this shoulder is barely visible, interrupting an otherwise monotonic decrease with increasing Z value.

TABLE I. Available excitation energy in MeV.

Beam target	C	Al	Ti	Cu
18 MeV/nucleon La	200	406	640	785
26 MeV/nucleon Xe	285	580	910	1110
31 MeV/nucleon Xe	340	690	1085	1325

On the other hand, the charge distribution is relatively flat for the reaction of 31 MeV/nucleon Xe + C, showing no signs of the peak observed at 26 MeV/nucleon around Z = 30. For the Xe + Al reaction, the distributions decreases with increasing Z value at low Z values, then becomes flat. For the heavier targets, the charge distribution strongly decreases with increasing Z value. The large increase in the yield of Z=10–15 for 31 MeV/nucleon again may indicate that at the higher center-of-mass energies, the emission of several fragments becomes the dominant exit channel. In such a picture, the average size of the fragments would then be reduced, the yield of the heavier fragments depleted, and the yield for the lighter fragments enhanced.

D. Coincidence data

There were a number of events in which fragments were observed in coincidence on either side of the beam. Higher-order coincidences were very rare due to their very low detection efficiency in the present experimental configuration, and there were essentially no events in which both fragments were detected on the same side of the

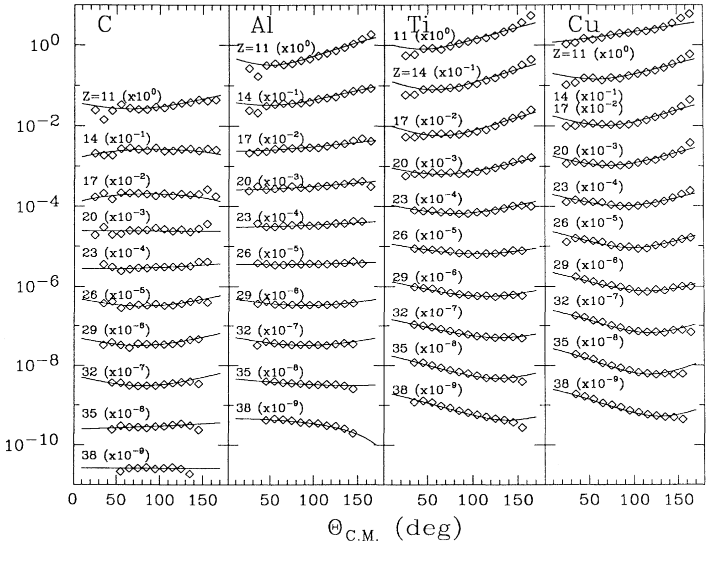

FIG. 5. Experimental angular distributions in the source frame for representative Z values produced in the reactions of ^{129}Xe + C, Al, Ti, and Cu. The solid curves represent the fitted functions that were used to extract the cross section for each Z value. Each column corresponds to a different target. The Z values, and a factor by which the data was multiplied for display purposes, are indicated to the left of each distribution.

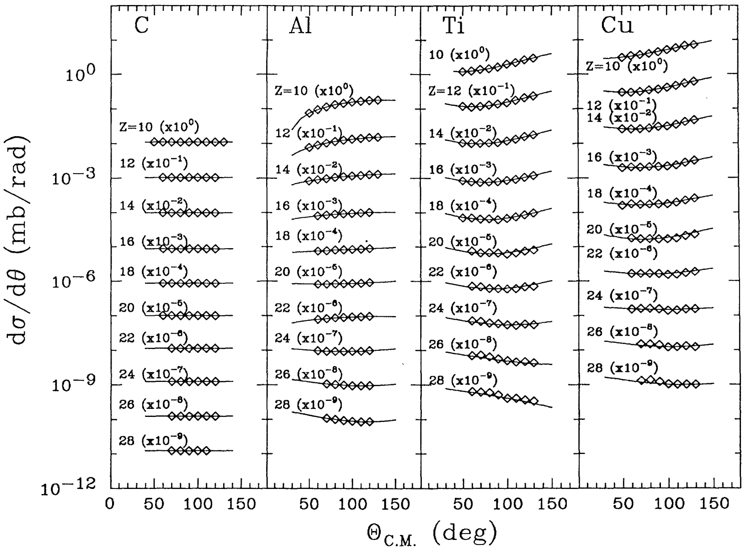

FIG. 6. Same as Fig. 5 but for 31 MeV/nucleon ^{129}Xe.

beam. For the coincidence events, the Z value of one fragment is shown as a function of the Z value of the second in Fig. 8. When a source with a constant total charge (Z_{total}) undergoes binary decay, coincidence events should lie along a line parallel to the equation

$$Z_1 + Z_2 = Z_{\text{total}}. \tag{2}$$

If there is a range of sources with different total nuclear charges that undergo binary decay, the events will no longer lie along a single line. Instead, there should be a broad band of events where the width of the total observed charge is related to the range of source sizes. For the very asymmetric reaction systems, most events fall within a narrow band that corresponds to an approximately constant sum of the two atomic numbers Z_1 and Z_2. There is some curvature of the $Z_1 + Z_2$ ridge visible in the 26 MeV/nucleon ^{129}Xe + C data. This could result from the preferential emission of charged particles from lower Z nuclei present in asymmetric splits of the compound nucleus (CN). With the heavier targets, in which incomplete fusion populates sources with a larger range of masses, the bands are much broader. These bands broaden even further with increasing bombarding energy. For the heaviest target at the highest bombarding energy, no distinct band is observed indicating the importance of events with more than two CF's in the exit channel. The

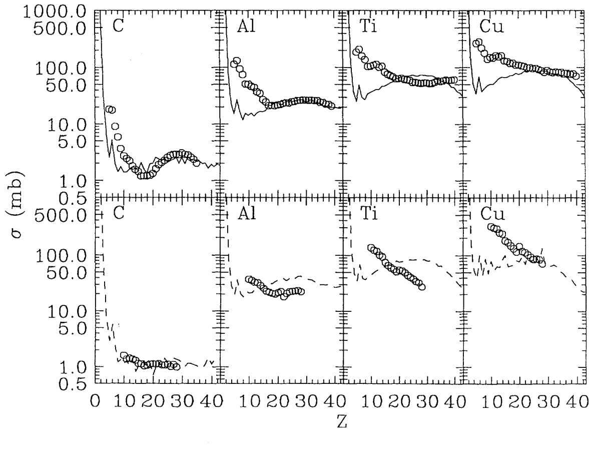

FIG. 7. Experimental angle-integrated cross sections as a function of a fragment Z value for 26 MeV/nucleon (upper row) and 31 MeV/nucleon (lower row) ^{129}Xe induced reactions. The solid and dashed lines are cross section predictions from the model. See discussion in text for details.

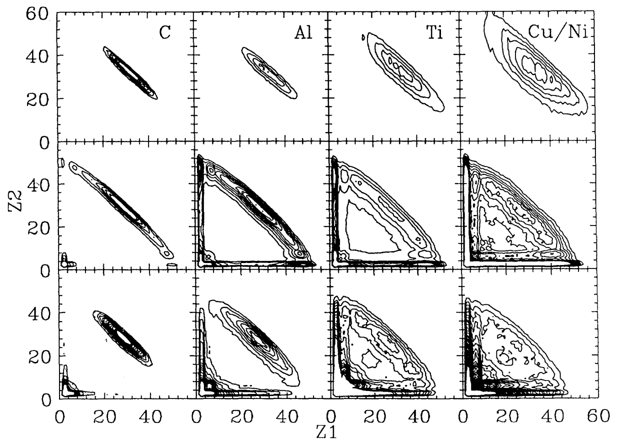

FIG. 8. Contour plots of the detected charge for twofold coincidence events from the 18 MeV/nucleon ^{139}La+X (top row), 26 MeV/nucleon ^{129}Xe+X (middle row), and 31 MeV/nucleon ^{129}Xe+X (bottom row) reactions. Z_1 and Z_2 refer to the Z value of each fragment detected. Each row corresponds to a different beam energy and each column to a different target. In column 4, a Ni target was used at 18 MeV/nucleon and a Cu target was used at the two higher beam energies. At 18 MeV/nucleon, the C and Al target data are from Ref. [6] and the Ti and Ni target data are from Refs. [37,8].

18 MeV/nucleon ^{139}La data are shown for comparison and were extracted from Refs. [6,8,37]. For the 26 and 31 MeV/nucleon reactions, the detector thresholds were low enough to detect alpha particles in coincidence with heavier complex fragments. Alpha-alpha and alpha-complex fragment coincidences can be observed as ridges parallel to the axes. The evolution from a narrow ridge for the very asymmetric entrance channels at low bombarding energy to a broad ridge which disappears for more symmetric reactions at higher bombarding energy follows the large increase in the available center-of-mass energy.

Histograms of Z_1+Z_2 are shown in Fig. 9 for reactions at 18, 26, and 31 MeV/nucleon. For the ^{129}Xe+C and ^{139}La+C reactions, the distributions are narrow. For the heavier targets, the distributions broaden and shift to lower Z values. In addition, a tail extending to low Z values develops. This is due to the incomplete detection of events in which there were more than two CF's in the exit channel. This tail becomes a substantial fraction of the total number of events at higher bombarding energies, where multibody exit channels may be prevalent. In constructing this figure, it was found to be useful to place a minimum Z threshold on each fragment to exclude alpha-CF and Z=6-CF ridges that can be seen in Fig. 8. This restriction is used to limit the contamination due to events in which one or more large fragments were not detected. The threshold was placed at Z=7 and this restriction is carried throughout the rest of the twofold event analysis. The dashed and dotted curves on this figure are the results from model calculations, which will be described later.

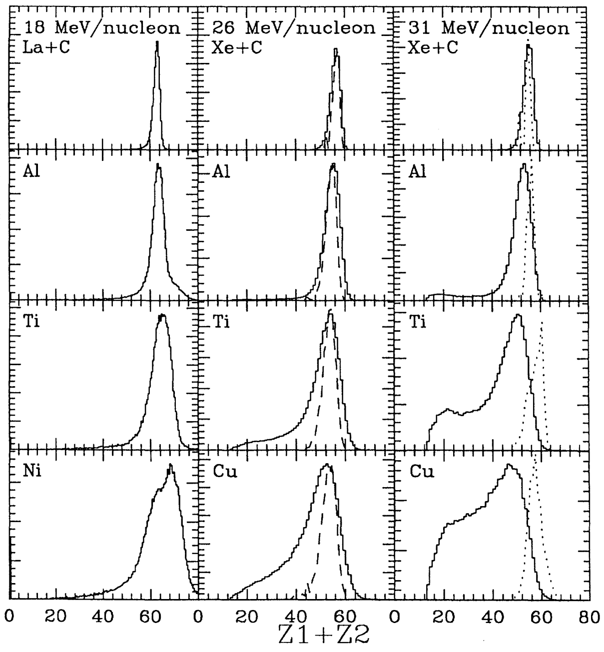

FIG. 9. The relative yield of coincidence events as a function of the total charge detected for column 1, the reaction of 18 MeV/nucleon ^{139}La+C, Al, and Ti, Ni; column 2, 26 MeV/nucleon ^{129}Xe+C, Al, Ti, and Cu; and column 3, 31 MeV/nucleon ^{129}Xe+C, Al, Ti, and Cu. The dashed and dotted curves are results from model calculations.

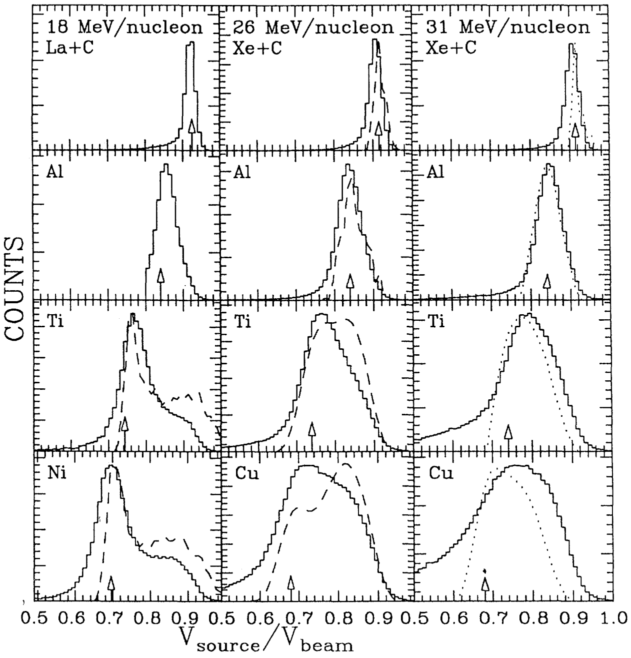

FIG. 10. The relative yield of coincidence events as a function of the calculated source velocity for column 1, the reaction of 18 MeV/nucleon ^{139}La+C, Al, Ti, and Ni; column 2, 26 MeV/nucleon ^{129}Xe+C, Al, Ti, and Cu; and column 3, 31 MeV/nucleon ^{129}Xe+C, Al, Ti, and Cu. Arrows indicate the complete fusion velocity for each system. The dashed curves and dotted curves are results from model calculations.

The center-of-mass velocity of the binary coincidence events was reconstructed for each event from the Z, total energy, Θ, and Φ of each fragment in the event. The distributions of the $V_{\parallel}$ component are shown in Fig. 10. The distributions in $V_{\perp}$ are very narrow. (The widths are given in Table II.) The arrows in Fig. 10 indicate the complete fusion velocity for each system. In the ^{129}Xe + C and Al reactions, only a peak corresponding to complete fusion or very near complete fusion is seen, similar to results observed for lower-energy reactions induced by ^{63}Cu, ^{93}Nb, and ^{139}La [7, 4, 6]. The data obtained for the reactions induced by 18 MeV/nucleon ^{139}La ions are shown for comparison. The dashed and dotted curves in this figure are the results from model calculations that are described below.

To obtain an overview of the evolution of the reaction with excitation energy, linear contour plots of the mea-

TABLE II. Perpendicular width of source velocity in units of v/c.

Beam target	C	Al	Ti	Cu
26 MeV/nucleon Xe	0.033	0.041	0.053	0.056
31 MeV/nucleon Xe	0.030	0.046	0.063	0.065

sured sum of the charges Z_1+Z_2 versus the derived emission source velocity for different target and beam energy combinations are shown in Fig. 11. An interesting evolution is observed with increasing target mass and beam energy. For the cases of the 14 and 18 MeV/nucleon ^{139}La + C, Al reactions [4] only narrow peaks corresponding to complete fusion are seen. However, for the 18 MeV/nucleon ^{139}La + Ni data [8], a band of events stretching from 90% of the beam velocity to the center-of-mass velocity occurs with the intensity peaked at the velocity corresponding to complete fusion. This band corresponds to the distribution of mass transfers expected for incomplete fusion [8]. One limit to the range of source velocities is given by small mass transfers in peripheral collisions. The resulting CN's will have very low excitation energy and are unlikely to decay by CF emission. These sources will have a velocity close to that of the beam. The other limit is given by complete fusion reactions which have a lower velocity and much higher excitation energy. A similar shape in the source velocity distribution is observed for the 18 MeV/nucleon ^{139}La + Ti reaction [37] and arises from the same mechanism. For the higher-energy 26 and 31 MeV/nucleon Xe + Ti and Cu reactions, a broad distribution of center-of-mass velocities is seen. The range in source velocities is again similar to that of the 18 MeV/nucleon data, but the Z_1+Z_2 distribution becomes broader, and the mean value decreases with increasing bombarding energy. This reflects the large amount of excitation energy available at higher bombarding energy and the correspondingly larger number of light charged particles evaporated from the hot primary fragments. The broad source velocity distribution indicates a broad range of mass transfers.

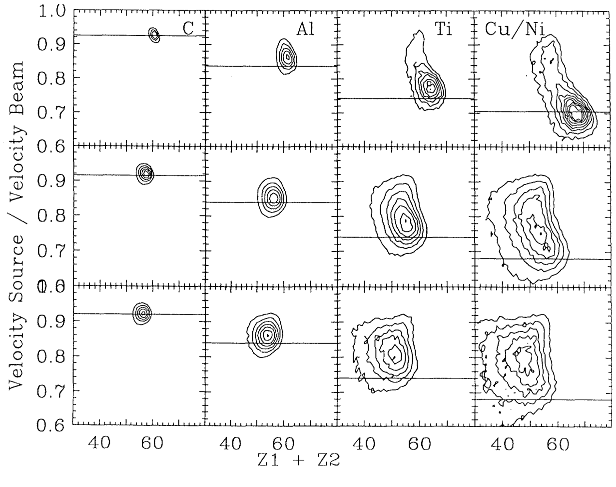

FIG. 11. Linearly spaced contours of source velocity vs total charge for twofold events from the 18 MeV/nucleon ^{139}La+X (top row), 26 MeV/nucleon ^{129}Xe+X (middle row), and 31 MeV/nucleon ^{129}Xe+X (bottom row) reactions. The data from 18 MeV/nucleon ^{139}La have been shifted down three units of Z to account for the difference in the La and Xe atomic numbers. The horizontal line is at the center-of-mass velocity for each system.

IV. INCOMPLETE FUSION MODEL

We have demonstrated that a large range of mass transfers leads to a distribution of source velocities in the reaction at 18 MeV/nucleon with the two heavier targets. The 18 MeV/nucleon ^{139}La + Ni data are consistent with an incomplete fusion reaction model [8]. To make a quantitative comparison with the data, we have used an incomplete fusion model [38] similar to the model of Dayras *et al.* [39]. In this model there are two stages: an incomplete fusion process followed by a statistical decay of the excited primary fragments. In the first stage, a geometrical incomplete fusion model is used to describe the dynamics of the reaction in which two sharp spheres represent the colliding nuclei. The energetics of fragment formation is assumed to be dominated by the increase in the surface area of the fragments. Since the surface area created by breaking a smaller nucleus into parts is less than the area created by breaking the larger nucleus into parts, it takes less energy to break the smaller target nucleus. To account for this, the model forces the overlapping nuclear matter to be sheared from the smaller target nucleus and fuses it onto the larger projectile nucleus to produce an excited compound nucleus plus a cold spectator. The model generates values for the Z, A, excitation energy, final spin J, and the laboratory velocity of each of the reaction partners. The excitation energy is calculated from the energetics of the surface creation and from the mass transfer. J is calculated from the relative motion of the centers of mass of the projectile and the lump of mass transferred from the target.

In the second stage, the primary fragments from the incomplete fusion model were allowed to statistically decay. The effect of the statistical deexcitation on the primary fragments was calculated using the statistical decay model (GEMINI) [4]. The statistical decay model simulates CF emission from the CN. GEMINI also models the center-of-mass energies and angles of emission of all fragments along the decay chain. The resulting events were then transformed into the laboratory to yield laboratory velocities and angles of the fragments. Finally, the fragments were passed through a detection filter that included the geometry and thresholds of the detectors used in the present study. The results are shown in the same figures as the experimental data. The only adjustable parameter in this model is the radius parameter (r_0) used to calculate the size of the sharp spheres (from $R = r_0 A^{1/3}$). The parameter r_0 was considered slightly adjustable to account for the fact that the model used a sharp-surfaced sphere to represent the nuclei, whereas in reality there is some diffuseness of the nuclear surface.

V. COMPARISON OF MODEL AND DATA

The results of the model calculations for 26 and 31 MeV/nucleon Xe + X reactions are shown in the Z_1+Z_2 versus V_{source} plane in Figs. 12 and 13. The top row of Fig. 12 depicts the experimental distributions from each of the four targets at 26 MeV/nucleon. The second, third, and fourth rows contain the model calculations for three different values of the sharp sphere radius parameter, r_0.

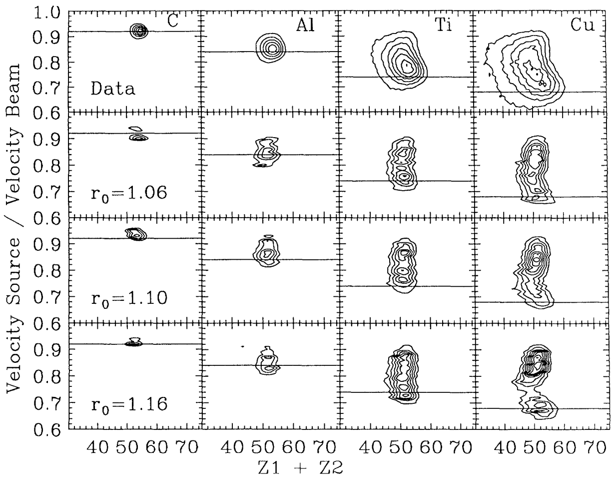

FIG. 12. Linearly spaced contours of source velocity vs total charge detected for twofold events from the 26 MeV/nucleon reactions. The top row is the data, while the next three rows are model calculations with values of r_0= 1.06, 1.10, and 1.16 fm, respectively.

Similar calculations with r_0 values of 1.10 fm and 1.16 fm are compared to the experimental distributions for the 31 MeV/nucleon systems in Fig. 13. The range of the source velocity and the position of the ridge in Z_1+Z_2 are qualitatively similar to the data for all systems. Note that there is little dependence on r_0 for the lighter C and Al systems. The model calculations for the heavy targets indicate a depletion of cross section in the region of intermediate to high mass transfers. For these events, the model predicts the resulting CN will decay into three or more CF's. The data for the same region indicate that there are a large number of events with no more than two CF's in the exit channel. In particular, the calculation shows a strong depletion for the Cu target at large r_0 at both bombarding energies which is not observed in the data. The width of the sum Z_1+Z_2 is much narrower from the model calculation than in the data.

The results from the model calculations with different r_0 values are compared to the data in the Z_1 versus Z_2 plane in the bottom three rows of Fig. 14 for the 26 MeV/nucleon reactions and in the bottom two rows of Fig. 15 for the 31 MeV/nucleon reaction. Little change is visible as a function of r_0 for the lighter targets. For the heavier Ti and Cu system, as r_0 is increased, the excitation energy in the model increases for a given center-of-mass velocity and this can be seen in the slightly increasing width of the Z_1 versus Z_2 distributions.

The calculation with an r_0 value of 1.10 fm gives the best agreement for the data at 26 MeV/nucleon. The source velocity distributions for the reactions of 18 MeV/nucleon ^{139}La+Ti,Ni were also calculated using an r_0 value of 1.10 fm and are shown in Fig. 9. The agreement of the calculation with the 18 MeV/nucleon data is very reasonable. The model predictions for all of the "observed" quantities, the cross sections, emission velocity, the width of the emission velocity, Z_1+Z_2, and source velocity for the reactions at 26 MeV/nucleon are compared with the data in Figs. 7, 4, 9, and 10, respectively. The overall agreement of the calculations with the 26 MeV/nucleon data is good for the lighter targets. For the heavier targets, the range of source velocities is correct (see Fig. 10) as is the centroid of the Z_1+Z_2 distribution (see Fig. 9) but the calculated width of the Z_1+Z_2 is narrower than that observed in the data. The inclusive cross sections (see Fig. 7) are well predicted for the lighter targets except for the low Z region. The sim-

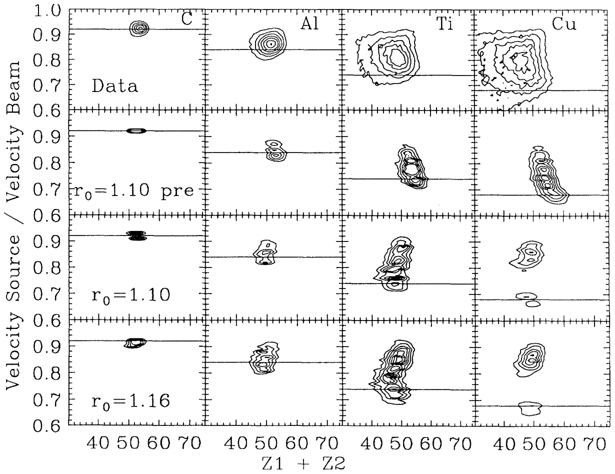

FIG. 13. Linearly spaced contours of source velocity vs total charge detected for twofold events from the 31 MeV/nucleon reactions. The top row is the data, the second row is a model calculation with preequilibrium included, while the bottom rows are model calculations with values of r_0= 1.10 and 1.16 fm, respectively.

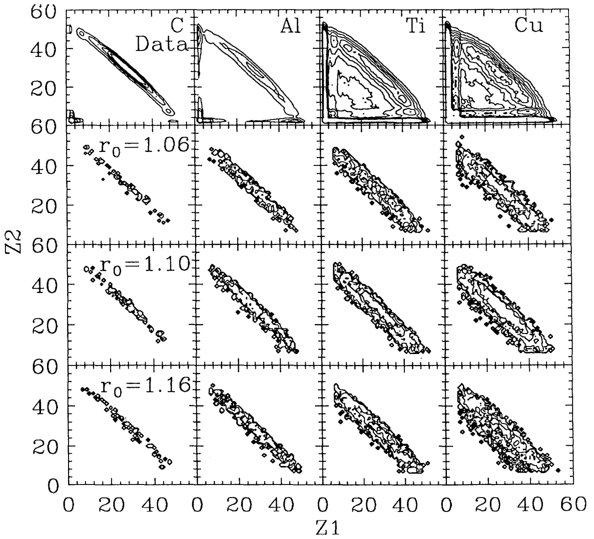

FIG. 14. Linearly spaced contour plots of the charge corelation for two-fold coincidence events from the 26 MeV/nucleon reactions. The top row is the data, while the next three rows are the results from model calculations. Details are given in the text.

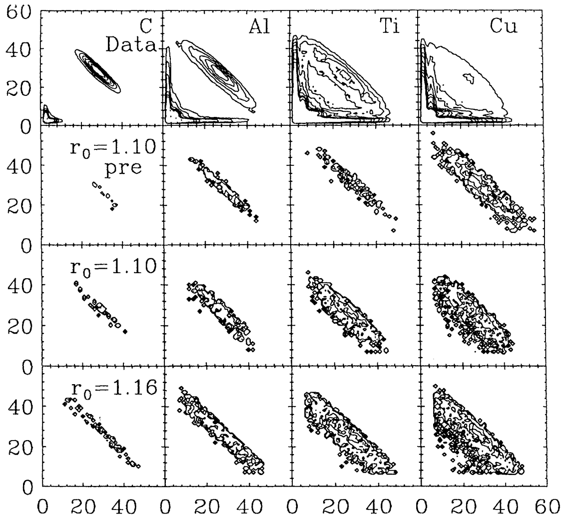

FIG. 15. Similar to Fig. 14 but for the 31 MeV/nucleon systems.

ulations for the heavier targets predict the correct order of magnitude but the shape of the cross section distributions is wrong. The calculated centroids and widths of the emission-velocity distributions agree well with the experimental data for all targets (see Fig. 4, upper row).

The 31 MeV/nucleon model calculations were not in as good agreement with the data as the 26 MeV/nucleon calculations for the heavier targets. This failing may be due to the overestimation of the excitation energy in the CN. Therefore a correction for preequilibrium emission was attempted. A Boltzman-Nordheim-Vlasov (BNV) model [40, 41] was used to estimate the amount of preequilibrium emission in the 31 MeV/nucleon reactions. The dynamical stage of the collision was simulated by solving the BNV equation with the test particle approach in a "full ensemble" method (each nucleon being represented by 50 test particles). The self-consistent mean field needed for the calculation included the Coulomb potential and a nuclear potential approximated by a density dependent Skyrme-like interaction. The parameters of the latter potential were chosen to reproduce nuclear matter saturation properties, and a compressibility coefficient of K=200 MeV. The free nucleon-nucleon cross section was used in the collision term with its energy and angular dependence. These are the same values used to reproduce ^{139}La + Al data at the somewhat higher energy of 55 MeV/nucleon [41]. The resulting average trajectory was followed until the slope of the emitted nucleon mean energy curve changed. This was taken to indicate the transition from preequilibrium emission to evaporation from a more equilibrated source.

The BNV code was run for the Xe + Al and Xe + Cu reactions at nearly central impact parameters leading to complete fusion. By comparing the BNV model results to those from the incomplete fusion model for the same impact parameter, the amount of nuclear charge, mass, excitation energy, and angular momentum lost in preequilibrium emission could be estimated. For the Al target, it was estimated that preequilibrium particles carried away 4 units of charge, 10 units of mass, 40% of the excitation energy, and 27% of the angular momentum. The uncertainties in these estimates are fairly large, being about 20% for each physical variable. At other impact parameters, the number of preequilibrium particles was scaled down to the amount of mass transfer predicted by the incomplete fusion model. The percentage of the angular momentum and excitation energy lost to preequilibrium emission was kept constant for all impact parameters. The calculation was repeated for the 26 MeV/nucleon and 18 MeV/nucleon reactions. For 26 MeV/nucleon, the calculation predicts only a small amount of preequilibrium emission and at 18 MeV/nucleon it predicts none. Because of the large uncertainties in these estimates, no corrections were attempted to the incomplete fusion model calculation at these two lower bombarding energies.

Figure 16 contains a comparison of the resulting primary fragments as a function of impact parameter for the 31 MeV/nucleon Xe+Al system. The solid lines are the results of the incomplete fusion model alone while the dashed lines are the results of the incomplete fusion model when including the effects of preequilibrium emission. At 31 MeV/nucleon, preequilibrium emission substantially reduces the excitation energy and to a lesser degree both the charge and angular momentum of the primary fragments. The results from the calculation which

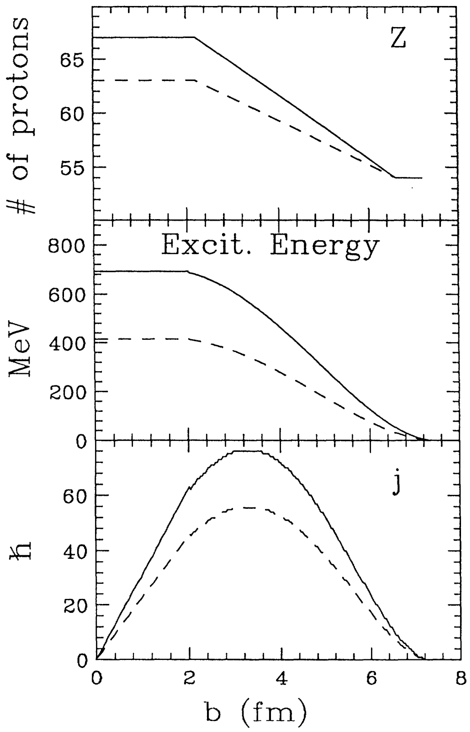

FIG. 16. A comparison between the input parameters for GEMINI for the ^{129}Xe+Al reaction from the incomplete fusion model (solid lines) and the parameters resulting from the BNV calculation (dashed lines) as a function of impact parameter.

included preequilibrium emission are shown in the second row of Figs. 13 and 15. The calculations for light targets remain in good agreement with the data. The depletion of events with moderate mass transfers for the Cu reaction no longer occurs and this model calculation is much closer to the observed V_{source} distributions. However, the peak value for Z_1+Z_2 is not well reproduced and the width of the Z_1+Z_2 distribution is again too narrow. (See the dotted curves in the last columns of Figs. 9 and 10.)

The predicted cross sections from the calculation including preequilibrium are shown as dashed curves in the lower row of Fig. 7. The cross section for the C and Al targets are well reproduced, however, for the heavier systems only the order of magnitude is correct and the shape of the distribution is not correct. The predictions from this calculation for the emission velocity and its width are shown as solid lines on the lower row of Fig. 4. The agreement between the calculation and the data is good. Since the agreement between the model calculation and data becomes significantly better after the inclusion of the preequilibrium emission, we conclude that there is a significant amount of preequilibrium emission in these reactions at 31 MeV/nucleon.

VI. SUMMARY

The production of complex fragments from the reactions of ^{129}Xe with C, Al, Ti, and Cu targets at 26 and 31 MeV/nucleon was measured. Angular distributions, emission velocities, source velocities, and cross sections were extracted from the data. The results were compared to a geometrical incomplete fusion model coupled to a statistical decay model. The 26 MeV/nucleon data were found to be well reproduced by this model with a radius parameter, r_0, equal to 1.10 fm. The results from reactions at 31 MeV/nucleon were also well described after a correction was made for preequilibrium emission. The agreement between the simple geometric incomplete fusion model and the data suggests that this model gives a reasonable description of the nuclear reactions in this energy region. The agreement also suggests that the complex fragments produced in this energy region arise from the compound nuclei produced in the incomplete fusion processes.

ACKNOWLEDGMENTS

One of us (K.H.) would like to thank the National Science Foundation for support under a NSF Graduate Fellowship. This work was supported in part by the National Science Foundation under Grant No. PHY-89-13815 and by the Director, Office of Energy Research, Office of High Energy and Nuclear Physics, Nuclear Physics Division, of the U.S. Department of Energy, under Contract No. AC03-76SF00098.

---

[1] L.G. Sobotka, M.L. Padgett, G.J. Wozniak, G. Guarino, A.J. Pacheco, L.G. Moretto, Y. Chan, R.G. Stokstad, I. Tserruya, and S. Wald, Phys. Rev. Lett. **51**, 2187 (1983).

[2] L.G. Sobotka, M.A. McMahan, R.J. McDonald, C. Signarbieux, G.J. Wozniak, M.L. Padgett, J.H. Gu, Z.H. Liu, Z.Q. Yao, and L.G. Moretto, Phys. Rev. Lett. **53**, 2004 (1984).

[3] M.A. McMahan, L.G. Moretto, M.L. Padgett, G.J. Wozniak, L.G. Sobotka, and M.G. Mustafa, Phys. Rev. Lett. **54**, 1995 (1985).

[4] R.J. Charity *et al.*, Nucl. Phys. **A483**, 371 (1988).

[5] H.Y. Han, K.X. Jing, E. Plagnol, D.R. Bowman, R.J. Charity, L. Vinet, G.J. Wozniak, and L.G. Moretto, Nucl. Phys. **A492**, 138 (1989).

[6] R.J. Charity *et al.*, Nucl. Phys. **A511**, 59 (1990).

[7] D.N. Delis *et al.*, Nucl. Phys. **A534**, 403 (1991).

[8] N. Colonna *et al.*, Phys. Rev. Lett. **62**, 1833 (1989).

[9] J.L. Wile *et al.*, Phys. Rev. C **45**, 2300 (1992).

[10] J.L. Wile *et al.*, Phys. Lett. B **264**, 26 (1991).

[11] F. Auger, B. Berthier, A. Cunsolo, A. Foti, W. Mittig, J.M. Pascaud, E. Plagnol, J. Quebert, and J.P. Wieleczko, Phys. Rev. C **35**, 190 (1987).

[12] R.J. Charity, D.R. Bowman, Z.H. Liu, R.J. McDonald, M.A. McMahan, G.J. Wozniak, L.G. Moretto, S. Bradley, W.L. Kehoe, and A.C. Mignerey, Nucl. Phys. **A476**, 516 (1988).

[13] R. Bougault *et al.*, Nucl. Phys. **A488**, 255c (1988).

[14] C. Chitwood, D.J. Fields, C.K. Gelbke, W.G. Lynch, A.D. Panagiotou, M.B. Tsang, H. Utsunomiya, and W.A. Freidman, Phys. Lett. **131B**, 289 (1983).

[15] B.V. Jacak, G.D. Westfall, C.K. Gelbke, L.H. Harwood, W.G. Lynch, D.K. Scott, H. Stoker, M.B. Tsang, and T.J.M. Symons, Phys. Rev. Lett. **51**, 1846 (1983).

[16] D.J. Fields, W.G. Lynch, C.B. Chitwood, C.K. Gelbke, M.B. Tsang, H. Utsunomiya, and J. Aichelin, Phys. Rev. C **30**, 1912 (1984).

[17] D.E. Fields *et al.*, Phys. Lett. B **220**, 356 (1989).

[18] M. Fatyga *et al.*, Phys. Rev. Lett. **58**, 2527 (1987).

[19] R. Bougault, D. Horn, C.B. Chitwood, D.J. Fields, C.K. Gelbke, D.R. Klesch, W.G. Lynch, M.B. Tsang, and K. Kwiatkowski, Phys. Rev. C **36**, 830 (1987).

[20] B. Borderie, M. Montoya, M.F. Rivet, D. Jouan, C. Cabot, H. Fuchs, D. Gardes, H. Gauvin, D. Jacquet, and F. Monnet, Phys. Lett. B **205**, 26 (1988).

[21] D.R. Bowman *et al.*, Nucl. Phys. **A523**, 386 (1991).

[22] P. Roussel-Chomaz *et al.*, Nucl. Phys. **A551**, 508 (1993).

[23] M.F. Rivet, B. Borderie, C. Gregoire, D. Jouan, and B. Remaud, Phys. Lett. B **215**, 55 (1988).

[24] Y.H. Chung, S.Y. Cho, and N.T. Porile, Nucl. Phys. **A533**, 170 (1991).

[25] T. Ethvignot *et al.*, Phys. Rev. C **43**, R2035 (1991).

[26] E. Plasecki *et al.*, Phys. Rev. Lett. **66**, 1291 (1991).

[27] Y. Blumenfeld *et al.*, Phys. Rev. Lett. **66**, 576 (1991).

[28] Y.D. Kin *et al.*, Phys. Rev. Lett. **67**, 14 (1991).

[29] D.R. Bowman *et al.*, Phys. Rev. Lett. **67**, 1527 (1991).

[30] R.T. de Souza *et al.*, Phys. Lett. B **268**, 6 (1991).

[31] B. Lott *et al.*, Phys. Rev Lett. **68**, 3141 (1992).

[32] J.R. Huizenga and W.U. Schroeder, Annu. Rev. Nucl. Part. Phys. **33**, 265 (1983).

[33] L.G. Moretto and G.J. Wozniak, Prog. Part. Nucl. Phys.

21, 401 (1991), and references therein.

[34] W.L. Kehoe, Ph.D. thesis, University of Maryland, 1989; University of Maryland Report No. DOE/ER/40321-5, 1989.

[35] D.R. Bowman, Ph.D. thesis, University of California at Berkeley, 1989; Lawrence Berkeley Laboratory Report No. LBL-27691, 1989.

[36] M.M. Fowler and R.C. Jared, Nucl. Instrum. Methods **124**, 341 (1975).

[37] N. Colonna (private communication).

[38] L.G. Moretto and D.R. Bowman, in *Proceedings of the Twenty-Fourth International Winter Meeting on Nuclear Physics,* Bormio, Italy, 1986, edited by I. Iori [Ric. Sci. Educ. Permanente, Suppl. **49**, 126 (1986)].

[39] R. Dayras *et al.,* Nucl. Phys. **A460**, 299 (1986).

[40] A. Bonasera, G.F. Burgio, and M. DiToro, Phys. Lett. B **221**, 233 (1989); A. Bonasera, G. Russo, and H.H. Wolter, *ibid.* **246**, 337 (1990).

[41] M. Colonna, P. Roussel-Chomaz, N. Colonna, M. Di Toro, L.G. Moretto, and G.J. Wozniak, Phys. Lett. B **283**, 180 (1992).